








Probing Nonequilibrium Dynamics of Photoexcited Polarons on a Metal-Oxide Surface with Atomic Precision

Chaoyu Guo (郭钊宇)^{1,2,*}, Xiangzhi Meng^{1,*†}, Huixia Fu^{3,*}, Qin Wang^{1,*}, Huimin Wang,³ Ye Tian,¹ Jinbo Peng¹,
Runze Ma¹, Yuxiang Weng³, Sheng Meng,^{3,4,‡} Enge Wang,^{1,3,4,5,§} and Ying Jiang^{1,4,5,¶}

¹International Center for Quantum Materials, School of Physics, Peking University, Beijing 100871, People's Republic of China

²Physical Science Laboratory, Huairou National Comprehensive Science Centre, Beijing 101400, People's Republic of China

³Institute of Physics, Chinese Academy of Sciences, Beijing 100190, People's Republic of China

⁴Collaborative Innovation Center of Quantum Matter, Beijing 100871, People's Republic of China

⁵CAS Center for Excellence in Topological Quantum Computation, University of Chinese Academy of Sciences, Beijing 100190, People's Republic of China

 (Received 7 September 2019; revised manuscript received 26 January 2020; accepted 9 April 2020; published 19 May 2020)

Understanding the nonequilibrium dynamics of photoexcited polarons at the atomic scale is of great importance for improving the performance of photocatalytic and solar-energy materials. Using a pulsed-laser-combined scanning tunneling microscopy and spectroscopy, here we succeeded in resolving the relaxation dynamics of single polarons bound to oxygen vacancies on the surface of a prototypical photocatalyst, rutile TiO₂(110). The visible-light excitation of the defect-derived polarons depletes the polaron states and leads to delocalized free electrons in the conduction band, which is further corroborated by *ab initio* calculations. We found that the trapping time of polarons becomes considerably shorter when the polaron is bound to two surface oxygen vacancies than that to one. In contrast, the lifetime of photogenerated free electrons is insensitive to the atomic-scale distribution of the defects but correlated with the averaged defect density within a nanometer-sized area. Those results shed new light on the photocatalytically active sites at the metal-oxide surface.

DOI: 10.1103/PhysRevLett.124.206801

Polarons, both in the perfect lattice and bound to defects, play a critical role in a wide spectrum of physicochemical properties of many metal oxides, such as photocatalysis [1], high- T_c superconductivity [2], thermoelectricity [3], and colossal magnetoresistance [4], to name just a few. In particular, taking a prototypical photocatalyst—titanium dioxide (TiO₂), for example—the formation of oxygen vacancies in metal oxides introduces excess electrons into the surrounding lattice, leading to polarons bound to the oxygen vacancies [5]. Such polarons are responsible for the localized states within the band gap, which extend the photoactivity of TiO₂ materials to the visible-light region [6–8] and are of great importance for improving the photoefficiency [9–11]. Although the ground-state polaron configurations have been well studied [12–14], it has been not possible to probe the nonequilibrium dynamics of photoexcited polaron states at the atomic scale [7,8,15–19], which is the key to achieving a microscopic understanding of various photoconversion processes.

Scanning tunneling microscopy (STM) and spectroscopy has proven to be an ideal tool for probing the structure and catalytic behaviors of individual defects and polarons on the TiO₂ surface with atomic resolution [9,10,20–24], but no transient dynamics information has been obtained so far due to the limitation of time resolution. By coupling the pulsed laser to the STM junction [25–29], here we were

able to track the trapping dynamics of individual polarons on a rutile TiO₂(110) surface by the oxygen vacancies and establish the direct correlation between the atomic environment and the photoresponse of polarons using a homemade cryogenic STM [Fig. 1(a)], which was optimized for optical pump-probe experiments at 5 K (see Fig. S1 [30]).

The stoichiometric rutile TiO₂(110) surface consists of alternating rows of hexacoordinated Ti_{6c} and pentacoordinated terminal Ti_{5c} aligned along the [001] crystallographic direction and linked by in-plane O_{ip} [Fig. 1(b)]. The adjacent Ti_{6c} are bridged by two-coordinated oxygen ions (O_b). The Ti_{5c} ions were imaged as bright rows along the [001] direction in the STM topography [Fig. 1(c)]. The surface O_b vacancy (V_O^{surf}) can be clearly distinguished, showing local segregation and a nanometer-sized density fluctuation.

The dI/dV spectrum taken at the defect-free area displays a wide band gap [“bkgd” in Fig. 1(d)], approaching the reported band gap value (3.0 eV) of the rutile TiO₂(110) surface [46]. The Fermi level (E_F) is very close to the conduction band minimum (CBM), indicating that our sample is highly reduced by V_O^{surf} . In contrast, the spectra taken around the V_O^{surf} show prominent in-gap states below the E_F , peaking around -1.1 eV [Fig. 1(d)]. Those in-gap states arise from the excess electrons introduced by

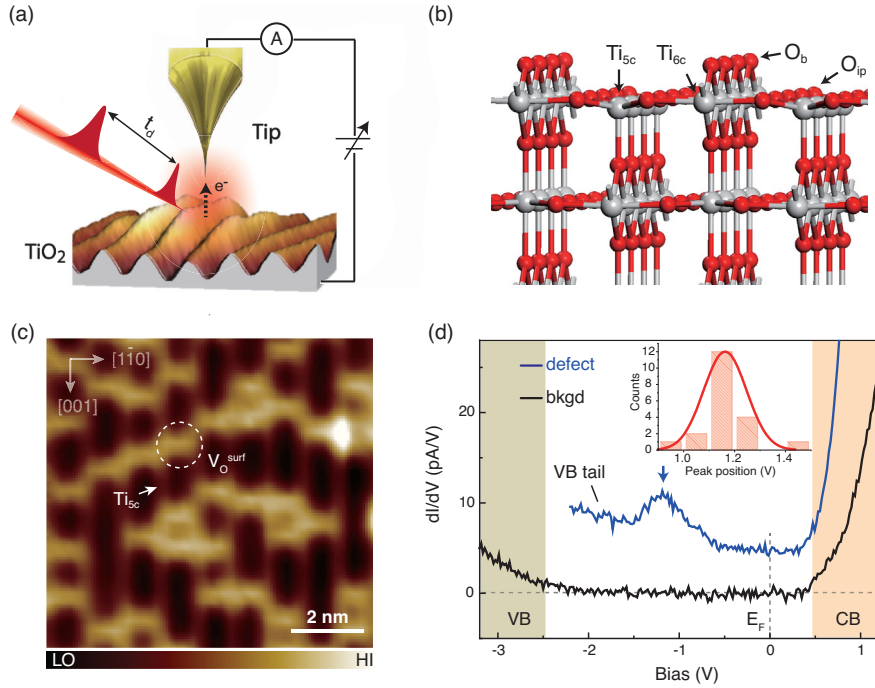


FIG. 1. In-gap state (polaron state) derived from the surface oxygen vacancies on $\text{TiO}_2(110)$. (a) Experimental setup of the laser-combined STM. (b) Atomic structure of the $\text{TiO}_2(110)$ surface. The hexacoordinated Ti (Ti_{6c}), pentacoordinated terminal Ti (Ti_{5c}), in-plane oxygen (O_{ip}), and bridge oxygen (O_b) are indicated. (c) STM topography of the $\text{TiO}_2(110)$ surface, where the surface O_b vacancy ($V_{\text{O}}^{\text{surf}}$) and Ti_{5c} row are denoted by the white dashed circle and white arrow, respectively. The set point of the STM image: $V = 1.7$ V and $I = 80$ pA. (d) dI/dV spectra taken around $V_{\text{O}}^{\text{surf}}$ and at the defect-free surface area (bkgd). Set points for $V_{\text{O}}^{\text{surf}}$ (1.7 V and $I = 200$ pA) and bkgd (1.7 V and $I = 30$ pA) were chosen differently to highlight the in-gap states. The spectrum of $V_{\text{O}}^{\text{surf}}$ was offset by 8 pA/V for clarity. The peak position of the polaron state is denoted by the blue arrow. The valence band (VB) and conduction band (CB) are represented by filled rectangles. The inset is the statistics of polaron energy distribution. Bin size, 100 mV. The red line represents the Gaussian (normal) curve fitting to the data.

oxygen vacancies and transferred to Ti ions near the $V_{\text{O}}^{\text{surf}}$ forming Ti^{3+} ions, which may therefore be considered as polarons bound to the $V_{\text{O}}^{\text{surf}}$ [5] (see Figs. S2 and S3 [30]). In fact, the energy of the polaron state displays a certain distribution within -0.9 to -1.4 eV, arising from the inhomogeneity of the local environment [inset in Fig. 1(d)]. The conduction band at the polaron site almost overlaps with that of the defect-free region (see Fig. S4 [30]), while a prominent tail near the valence band maximum (VBM) appears accompanied with the polaron state. Such tail states in dI/dV spectra may correspond to the multiple phonon sidebands due to the vibronic coupling [38].

The topography and the density of states (DOS) distribution of a single $V_{\text{O}}^{\text{surf}}$ are shown in Figs. 2(a) and 2(b), respectively. It is obvious that the $V_{\text{O}}^{\text{surf}}$ -derived polaron states are mainly distributed at four lobes surrounding the $V_{\text{O}}^{\text{surf}}$ [see the white arrows in Fig. 2(b)] but with different weights. This asymmetry in the DOS intensity may result from kinetic trapping of the polarons in one of a number of nearly degenerate ground-state configurations [12]. The polaron hopping is constrained around $V_{\text{O}}^{\text{surf}}$ because of its electrostatic attraction with the positively charged $V_{\text{O}}^{\text{surf}}$ and the stronger el-ph coupling near the $V_{\text{O}}^{\text{surf}}$ (see Table S1 [30]).

Statistical analysis reveals that the density of polarons is close to twice that of $V_{\text{O}}^{\text{surf}}$ (see Fig. S5 [30]), since each oxygen vacancy donates two excess electrons. Although the two excess electrons are believed to populate preferentially the subsurface Ti_{6c} under the Ti_{5c} sites according to the *ab initio* calculations [12] [Fig. 2(d)], their wave functions can still extend to the surface Ti_{5c} , thus allowing the STM imaging.

First, we studied the photoexcitation of polaron states in the steady state by illuminating the STM junction with a quasicontinuous laser (single path). In order to focus on the photoresponse of the in-gap polaron states, we applied the below-band-gap excitation (wavelength >500 nm). The results are shown in Fig. 2(c). The energy of polaron states exhibits a clear downward shift under the 700-nm laser illumination. In addition, a considerable suppression of the VB tail states and an upward shift of the CB edge can be also found.

Such energetic shifts of defect states and the band edges might have several possible origins. First, it can be caused by the surface photovoltage [47]. However, we found that the high doping level of the sample leads to negligible band bending near the $\text{TiO}_2(110)$ surface [48] (see Fig. S6 [30]).

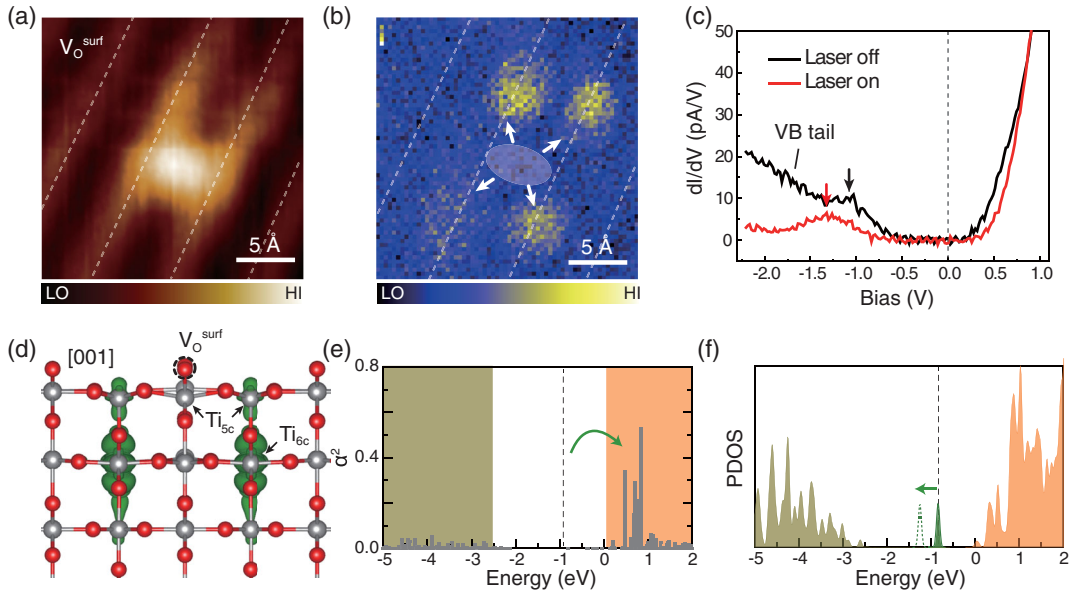


FIG. 2. The photoexcitation of a single polaron. (a),(b) The topography and dI/dV mapping of $V_{\text{O}}^{\text{surf}}$. The white dashed lines highlight the Ti_{5c} rows. In (b), the filled ellipse denotes the $V_{\text{O}}^{\text{surf}}$ site, and the white arrows indicate the distribution of the polaron states. Set points of STM topography and dI/dV mapping: $V = 1.7$ V and $I = 70$ pA (a),(b). The dI/dV mapping was acquired with an open feedback loop at the bias: $V = -1.2$ V. The red (black) curves in (c) show the dI/dV spectra with (without) the 700-nm laser irradiation. Laser power, 2 mW. The arrows mark the peak positions of polaron states. Set point: $V = 1.7$ V and $I = 100$ pA. (d) Optimized structure of one $V_{\text{O}}^{\text{surf}}$ on rutile (110) surface and the excess electron distribution. The excess electron density is highlighted by dark green, and the value of the isosurface is 10^{-2} electrons/ \AA^3 . Gray and red spheres are the Ti and O ions, respectively. (e) The strength of optical transition probability between the defect state and the states in the VB and CB. Here α is the transition dipole moment between the defect state and VB or CB states. The zero energy was set at the CBM. The curved arrows denote the direction of the charge transfer. (f) The projected DOS of defect states for $V_{\text{O}}^{\text{surf}}$ before (filled) and after (dashed) the charge transfer ($0.2e$). The arrows denote the shift of the defect states. The dashed vertical lines denote the position of defect levels.

Second, the laser-induced heating effect may also induce the change of defect states because of the lattice relaxation [49]. We have carried out bias polarity and laser polarization-dependent experiments to exclude this possibility (see Fig. S7 [30]). Third, the optical Stark effect can be neglected considering the small electronic dipole moment induced by the photoexcitation and the small electric field of the pulsed laser [50]. Therefore, the most possible origin of the changes in dI/dV spectra under laser illumination then points to the photoinduced electronic transition between the polaron states and CB or VB. To substantiate this assumption, we performed systematic *ab initio* density functional theory calculations [Fig. 2(d)] (see Materials and Methods for details [30]). We first calculated the transition dipole moment between the polaron states and the CB or VB [Fig. 2(e)]. It is interesting that the electronic transition from the in-gap states to CB states is preferred, whereas the transition dipole between the in-gap state and the VB states is very small. A more detailed analysis shows that such a transition propensity is closely related to the strong wave function overlap between the in-gap state and Ti orbitals comprising the conduction band.

To simulate the photoexcitation effects, we analyze the electronic structure of the TiO_2 surface by artificial

population inversion: removing electrons from the in-gap states and filling into the conduction band self-consistently. Upon the electron transfer, the in-gap states exhibit a distinct downward shift [Fig. 2(f)], which nicely reproduces the experimental observations [Fig. 2(c)]. Such an energetic shift mainly originates from the decrease of the on-site Coulomb interaction energy (U) when the electrons are removed from the in-gap states. The suppression of the VB tail and the shift of the CB edge under the photoexcitation [Fig. 2(c)] can then be attributed to the depletion of the polaron states and the accumulation of the free electrons in the CBM, respectively (see Fig. S8 [30]).

So far, all the photo-STM measurements were done in the steady state, which involves a dynamic balance between the excitation and deexcitation of the defect-bound polaron states. When an electron is photoexcited from the polaron state to the conduction band, it can migrate away from the oxygen vacancy site and form a new polaron in the defect-free region. Those polarons are free to hop on the surface and can be finally trapped by the oxygen vacancies again. In order to extract the trapping dynamics of the polaron states, we carried out pump-probe experiments based on the STM setup using two 532-nm nanosecond pulsed lasers (Figs. S9 and S10 [30]). The interference from

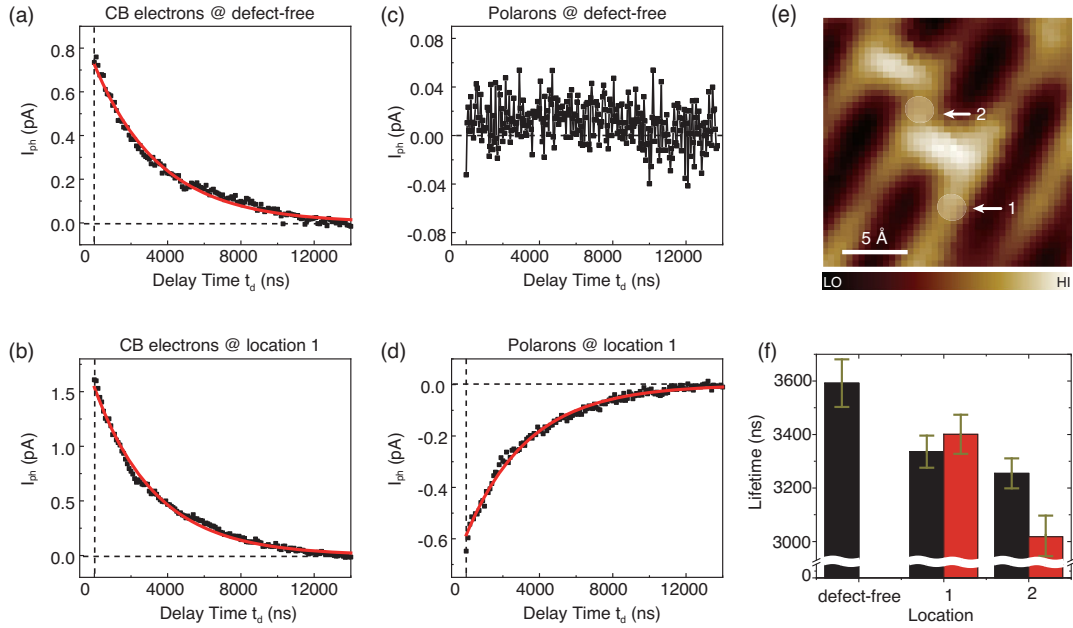


FIG. 3. Spatially dependent lifetimes of photoexcited electrons and polaron states. (a),(b) and (c),(d) Photoinduced current I_{ph} versus delay time t_d between the two 532-nm laser pulses arising from the photoexcited electrons in the CB and the photodepletion of polarons, respectively. The red lines represent the exponential fitting to the data. Set points: $V = 1.7$ V and $I = 80$ pA (a),(b), $V = -2.2$ V and $I = 2$ pA (c), and $V = -1.7$ V and $I = 50$ pA (d). Laser power, 0.1 mW. The result in (c) has the identical relative resolution as that in (d) although the set point is about a factor of 10 lower. (e) The topography of a V_O^{surf} dimer. The filled circles denote the position of two ground-state polarons, where polaron 1 is isolated and polaron 2 is bound to two defects. (a),(c) and (b),(d) were taken at defect-free region and defect site [location 1 in (e)], respectively. (f) Location dependence of the lifetimes for photoexcited electrons and polarons, which were extracted from the exponential fitting of $I_{ph}(t_d)$ curves. The error bars arise from the fitting error.

transient thermal expansion of the tip can be suppressed by carefully adjusting the polarization, power, and focus of the laser (Fig. S11 [30]).

The relaxation dynamics of photoexcited polaron states and free electrons in the CB at different sites is shown in Fig. 3. When the bias was set at the CB edge, we observed a perfect exponential decay in the photoinduced tunneling current (I_{ph}) versus the delay time between the two laser pulses (t_d) for both the defect-free area [Fig. 3(a)] and polaron sites [Fig. 3(b)], reflecting the decay dynamics of the photogenerated electrons at CBM. The fitted lifetime yields several microseconds, which is considerably larger than the optical results obtained on the rutile $TiO_2(110)$ [51]. Such a discrepancy might arise from the far lower temperature in the present measurement (5 K). In contrast, the I_{ph} measured at the VB tail [see Fig. 1(d)] reveals the relaxation dynamics of the polarons. It shows negligible signals at the defect-free areas [Fig. 3(c)] but exhibits an inverse decay behavior at the polaron sites [Fig. 3(d)]. It suggests that we do not measure the formation time of a polaron in the perfect TiO_2 lattice (typically on the order of femtoseconds to picoseconds) [52,53] but the time for the free polarons to be trapped by the oxygen vacancies, which shows significant temperature dependence.

Interestingly, the lifetime of the photoexcited polaron states relies on their local environments [Figs. 3(e) and 3(f)].

When two oxygen vacancies are close to each other such that the polaron state is simultaneously bound to the two V_O^{surf} defects [location 2 in Fig. 3(e)], its lifetime becomes much shorter than that of the isolated case [location 1 in Fig. 3(e)]. It suggests that the defect aggregation may facilitate the trapping of the polarons due to the deeper potential well formed by lattice distortion. We found that, once the separation of the polarons is larger than 0.5 nm, the timescale of polaron dynamics becomes the same as that of the isolated polaron, which is consistent with the nature of small polarons at the rutile $TiO_2(110)$ surface [12]. However, the lifetime of the electrons is less sensitive to the atomic-scale aggregation of the defects. Such a difference can be rationalized by the spatially delocalized nature of free electrons in the CB.

We found that the lifetime of photogenerated electrons exhibits more prominent dependence on the nanoscale density fluctuation of the defects (Fig. 4). We first scanned a certain area (20×20 nm²) and then calculated the averaged defect density. The lifetime of different areas decreases by a factor of 3 as the averaged density of the oxygen vacancies increases by $\sim 30\%$. However, within the same area, the lifetime shows very small spatial dependence and varies only by 8%. Although the distribution of the defects exhibits strong atomic-scale inhomogeneity [see the insets in Fig. 4], the photogenerated free electrons seem

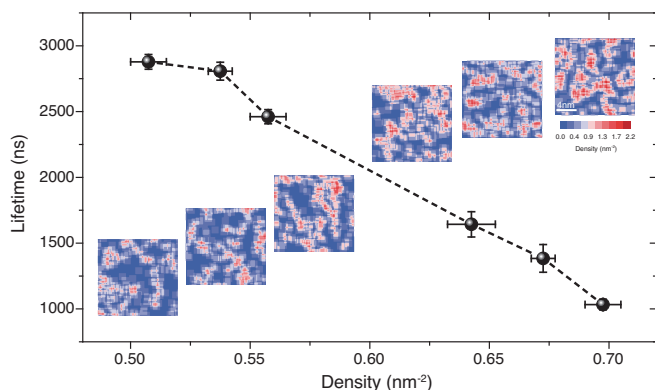


FIG. 4. The lifetimes of photoexcited free electrons in the CB as a function of the defect density. The lifetimes were extracted from the $I_{\text{ph}}(t_d)$ spectra taken at defect-free regions. Set points: $V = 1.7$ V and $I = 100$ pA. Laser power, 0.1 mW. The averaged defect density was calculated within 20×20 nm² areas. The error bars of the lifetime and the defect density reflect the fitting error and the statistical error, respectively. The insets are the defect density mapping of six 20×20 nm² areas with the averaged defect density ranging from 0.51/nm² to 0.70/nm². The local density was analyzed in square areas of 1.8×1.8 nm², which defines the resolution of the density mapping.

to overlook it. Notably, the electron lifetime shows a nearly linear relation on the local defect density, which might be related to the diffusion length of CB electrons [54,55]. Those free electrons diffuse over this area in an ergodic way and are frequently scattered by the oxygen defects. Therefore, the probability for free electrons to be trapped by the oxygen defects (lifetime) should be proportional to the defect density.

In summary, this work provides the first spatiotemporal information for the relaxation dynamics of photoexcited single polarons, which reveals the critical role of atomic environments. We found that the visible-light excitation of the polarons bound to surface oxygen vacancies leads to depletion of the polaron states and delocalized free electrons in the conduction band. The polaron trapping becomes considerably faster when the polaron is bound to two surface oxygen vacancies than that to one, suggesting that such a shared polaron site could have enhanced catalytic activity. This may modify the conventional picture of photocatalytically active sites at the metal-oxide surface and provide new guides for defect engineering of photocatalytic materials. In addition, the lifetime of photogenerated free electrons is insensitive to the atomic-scale distribution of the defects but correlated to the averaged defect density within tens of nm² area. Such findings have particular implications for metal-oxide nanoparticles with nanometer-sized facets, whose photocatalytic performance may differ from one to another due to the nanoscale spatial inhomogeneity of the oxygen vacancies.

This work was supported by the National Key R&D Program under Grants No. 2016YFA0300901,

No. 2016YFA0300902, and No. 2017YFA0205003, the National Natural Science Foundation of China under Grants No. 11888101, No. 21725302, No. 11634001, No. 11934003, and No. 91850120, the Strategic Priority Research Program of Chinese Academy of Sciences under Grant No. XDB28000000, and Beijing Municipal Science & Technology Commission under Grant No. Z191100007219005.

*These authors contributed equally to this work.

[†]Present address: Physikalisches Institut, Westfälische Wilhelms-Universität, Wilhelm-Klemm-straße10, 48149 Münster, Germany.

[‡]smeng@iphy.ac.cn

[§]egwang@pku.edu.cn

[¶]yjiang@pku.edu.cn

- [1] S. D. Jackson and J. S. J. Hargreaves, *Metal Oxide Catalysis* (Wiley, Weinheim, 2008).
- [2] E. Salje, A. S. Alexandrov, and W. Y. Liang, *Polarons and Bipolarons in High-Tc Superconductors and Related Materials* (Cambridge University Press, Cambridge, England, 2005).
- [3] M. Wang, C. Bi, L. Li, S. Long, Q. Liu, H. Lv, N. Lu, P. Sun, and M. Liu, *Nat. Commun.* **5**, 4598 (2014).
- [4] H. M. Rønnow, C. Renner, G. Aeppli, T. Kimura, and Y. Tokura, *Nature (London)* **440**, 1025 (2006).
- [5] A. L. Shluger, K. P. McKenna, P. V. Sushko, D. M. Ramo, and A. V. Kimmel, *Model. Simul. Mater. Sci. Eng.* **17**, 084004 (2009).
- [6] C. M. Yim, C. L. Pang, and G. Thornton, *Phys. Rev. Lett.* **104**, 036806 (2010).
- [7] F. Zuo, L. Wang, T. Wu, Z. Y. Zhang, D. Borchardt, and P. Y. Feng, *J. Am. Chem. Soc.* **132**, 11856 (2010).
- [8] A. Naldoni, M. Allieta, S. Santangelo, M. Marelli, F. Fabbri, S. Cappelli, C. L. Bianchi, R. Psaro, and V. Dal Santo, *J. Am. Chem. Soc.* **134**, 7600 (2012).
- [9] U. Diebold, *Surf. Sci. Rep.* **48**, 53 (2003).
- [10] M. A. Henderson, *Surf. Sci. Rep.* **66**, 185 (2011).
- [11] Q. Guo, C. Y. Zhou, Z. B. Ma, Z. F. Ren, H. J. Fan, and X. M. Yang, *Chem. Soc. Rev.* **45**, 3701 (2016).
- [12] C. M. Yim, M. B. Watkins, M. J. Wolf, C. L. Pang, K. Hermansson, and G. Thornton, *Phys. Rev. Lett.* **117**, 116402 (2016).
- [13] M. Reticioli, M. Setvin, X. F. Hao, P. Flauger, G. Kresse, M. Schmid, U. Diebold, and C. Franchini, *Phys. Rev. X* **7**, 031053 (2017).
- [14] M. Reticioli, I. Sokolovic, M. Schmid, U. Diebold, M. Setvin, and C. Franchini, *Phys. Rev. Lett.* **122**, 016805 (2019).
- [15] Z. Q. Wang *et al.*, *J. Am. Chem. Soc.* **137**, 9146 (2015).
- [16] S. Moser *et al.*, *Phys. Rev. Lett.* **110**, 196403 (2013).
- [17] A. Argondizzo, S. J. Tan, and H. Petek, *J. Phys. Chem. C* **120**, 12959 (2016).
- [18] M. Zhu, Y. Mi, G. B. Zhu, D. Y. Li, Y. P. Wang, and Y. X. Weng, *J. Phys. Chem. C* **117**, 18863 (2013).
- [19] N. G. Petrik and G. A. Kimmel, *J. Phys. Chem. C* **115**, 152 (2011).
- [20] T. Minato *et al.*, *J. Chem. Phys.* **130**, 124502 (2009).
- [21] S. Wendt *et al.*, *Science* **320**, 1755 (2008).

- [22] M. Setvin, U. Aschauer, P. Scheiber, Y.-F. Li, W. Hou, M. Schmid, A. Selloni, and U. Diebold, *Science* **341**, 988 (2013).
- [23] O. Bikondoa, C. L. Pang, R. Ithnin, C. A. Muryn, H. Onishi, and G. Thornton, *Nat. Mater.* **5**, 189 (2006).
- [24] M. Setvin, M. Wagner, M. Schmid, G. S. Parkinson, and U. Diebold, *Chem. Soc. Rev.* **46**, 1772 (2017).
- [25] Y. Terada, S. Yoshida, O. Takeuchi, and H. Shigekawa, *Nat. Photonics* **4**, 869 (2010).
- [26] P. Kloth and M. Wenderoth, *Sci. Adv.* **3**, e1601552 (2017).
- [27] T. L. Cocker, V. Jelic, M. Gupta, S. J. Molesky, J. A. J. Burgess, G. De Los Reyes, L. V. Titova, Y. Y. Tsui, M. R. Freeman, and F. A. Hegmann, *Nat. Photonics* **7**, 620 (2013).
- [28] T. L. Cocker, D. Peller, P. Yu, J. Repp, and R. Huber, *Nature (London)* **539**, 263 (2016).
- [29] S. W. Li, S. Y. Chen, J. Li, R. Q. Wu, and W. Ho, *Phys. Rev. Lett.* **119**, 176002 (2017).
- [30] See Supplemental Material at <http://link.aps.org/supplemental/10.1103/PhysRevLett.124.206801> for details of additional data, discussions, figures, and a table, which includes Refs. [25,26,31–45].
- [31] G. Kresse and J. Furthmüller, *Phys. Rev. B* **54**, 11169 (1996).
- [32] J. P. Perdew, K. Burke, and M. Ernzerhof, *Phys. Rev. Lett.* **77**, 3865 (1996).
- [33] C. F. Craig, W. R. Duncan, and O. V. Prezhdo, *Phys. Rev. Lett.* **95**, 163001 (2005).
- [34] A. V. Akimov and O. V. Prezhdo, *J. Chem. Theory Comput.* **9**, 4959 (2013).
- [35] J. Zhang, H. Hong, J. Zhang, H. Fu, P. You, J. Lischner, K. Liu, E. Kaxiras, and S. Meng, *Nano Lett.* **18**, 6057 (2018).
- [36] R. Long, N. J. English, and O. V. Prezhdo, *J. Am. Chem. Soc.* **134**, 14238 (2012).
- [37] S. K. Gautam, F. Singh, I. Sulania, R. G. Singh, P. K. Kulriya, and E. Pippel, *J. Appl. Phys.* **115**, 143504 (2014).
- [38] S. W. Wu, G. V. Nazin, X. Chen, X. H. Qiu, and W. Ho, *Phys. Rev. Lett.* **93**, 236802 (2004).
- [39] X. Yin, H. M. Chen, F. H. Pollak, Y. Chan, P. A. Montano, P. D. Kirchner, G. D. Pettit, and J. M. Woodall, *Appl. Phys. Lett.* **58**, 260 (1991).
- [40] Q. Liu, C. Chen, and H. Ruda, *J. Appl. Phys.* **74**, 7492 (1993).
- [41] Y. Terada, S. Yoshida, O. Takeuchi, and H. Shigekawa, *J. Phys. Condens. Matter* **22**, 264008 (2010).
- [42] H. Shigekawa, O. Takeuchi, and M. Aoyama, *Sci. Technol. Adv. Mater.* **6**, 582 (2005).
- [43] M. Yamashita, H. Shigekawa, and R. Morita, *Mono-Cycle Photonics and optical Scanning Tunneling Microscopy: Route to Femtosecond Ångstrom Technology* (Springer Science & Business Media, New York, 2005), Vol. 99.
- [44] R. Huber, M. Koch, and J. Feldmann, *Appl. Phys. Lett.* **73**, 2521 (1998).
- [45] P. Kloth, T. Thias, O. Bunjes, J. von der Haar, and M. Wenderoth, *Rev. Sci. Instrum.* **87**, 123702 (2016).
- [46] M. Gratzel, *Nature (London)* **414**, 338 (2001).
- [47] L. Kronik and Y. Shapira, *Surf. Sci. Rep.* **37**, 1 (1999).
- [48] Z. Zhang and J. T. Yates, *Chem. Rev.* **112**, 5520 (2012).
- [49] T. Sekiya, T. Yagisawa, N. Kamiya, D. Das Mulmi, S. Kurita, Y. Murakami, and T. Kodaira, *J. Phys. Soc. Jpn.* **73**, 703 (2004).
- [50] L. Sun, A. Dong, J. Li, D. Hao, X. Tang, S. Yan, Y. Guo, X. Shan, and X. Lu, *Phys. Rev. B* **98**, 081402 (2018).
- [51] K. Ozawa, M. Emori, S. Yamamoto, R. Yukawa, S. Yamamoto, R. Hobara, K. Fujikawa, H. Sakama, and I. Matsuda, *J. Phys. Chem. Lett.* **5**, 1953 (2014).
- [52] B. Li, J. Zhao, K. Onda, K. D. Jordan, J. Yang, and H. Petek, *Science* **311**, 1436 (2006).
- [53] J. Schneider, M. Matsuoka, M. Takeuchi, J. Zhang, Y. Horiuchi, M. Anpo, and D. W. Bahnemann, *Chem. Rev.* **114**, 9919 (2014).
- [54] Y. Yamada and Y. Kanemitsu, *Appl. Phys. Lett.* **101**, 133907 (2012).
- [55] H. Frederiksen, *J. Appl. Phys.* **32**, 2211 (1961).